Environment and Natural Resources Journal

Volume 25
Issue X
2027

# Impact of Biomass Burning Aerosols on Warm Cloud Microphysics and Rain Suppression in Northern Thailand

**Pakdee Chantraket[1*] and Sritam Danpradit[2]**

*[1]Cooperative Promotion Department, Ministry of Agriculture and Cooperatives, Bangkok, Thailand*
*[2]Department of Royal Rainmaking and Agricultural Aviation, Ministry of Agriculture and Cooperatives, Bangkok, Thailand*

## ARTICLE INFO

Received: 31 Dec 2025
Received in revised: 10 Sep 2026
Accepted: 14 Sep 2026
Published online: 16 Nov 2026
DOI: 10.32526/ennrj/25/20250393

**Keywords:**
Aerosols pollution/ Warm cloud microphysics/ Rain suppression/ Northern Thailand

*** Corresponding author:**
E-mail: pakdee2@gmail.com

## ABSTRACT

This study investigates the microphysical properties and temporal evolution of warm cumulus clouds over Northern Thailand during the biomass burning season. In-situ measurements were conducted using a research aircraft equipped with full-spectrum aerosol and cloud probes (UHSAS, PCASP, FSSP). The observations reveal distinct aerosol signatures: fresh plumes dominated by the Aitken mode (<0.1 µm) and aged plumes characterized by the accumulation mode (0.1-0.3 µm). Despite high Cloud Condensation Nuclei (CCN) loading, cloud droplet growth was severely suppressed. In-cloud measurements showed narrow droplet size distributions with a sharp cutoff at 15-18 µm, preventing the onset of collision-coalescence. Temporal tracking of cloud turrets ($\Delta t \approx 20$ min) revealed a dominant trend of rapid dissipation, with Liquid Water Content (LWC) decreasing by 30-60% due to dry air entrainment. An extreme "cloud choking" event was observed where massive aerosol intrusion (concentration >7,000 $cm^{-3}$) accelerated evaporation via the semi-direct effect. These findings indicate that high aerosol loading in this region not only suppresses precipitation initiation but also shortens cloud lifetime.

## HIGHLIGHTS

- In-situ aircraft observations revealed distinct aerosol regimes, with fresh plumes dominated by Aitken-mode and aged plumes by accumulation-mode aerosols.
- High CCN loading suppressed droplet growth, limiting sizes to 15-18 µm and inhibiting collision-coalescence.
- High aerosol loading combined with dry air entrainment cause by a rapid 30-60% loss in liquid water content, leading to rapid cloud dissipation.
- Extreme aerosol concentrations triggered a "cloud choking" effect that accelerates evaporation and substantially shortens the overall lifetime of warm cumulus clouds.

## 1. INTRODUCTION

Biomass burning in Southeast Asia is a major source of atmospheric aerosols, particularly during the dry season (February to April) (Luong et al., 2022; Jainontee et al., 2023; Saksakulkrai et al., 2023). The intensive emission of carbonaceous particles from agricultural residues and forest fires leads to severe haze episodes over Northern Thailand (Sresawasd et al., 2021; Amnuaylojaroen et al., 2020; Kawichai et al., 2024). This spatial accumulation is heavily governed by the region's complex topography, which is characterized by deep intermontane basins in northern Thailand (Inlaung et al., 2024; Bran et al., 2024). During the dry season, the high surrounding mountain ranges, combined with strong thermal inversions, act as a physical barrier, trapping biomass burning plumes and aerosols within the lower boundary layer. These aerosols serve as Cloud Condensation Nuclei (CCN), significantly altering cloud microphysical properties and precipitation efficiency (Chen et al., 2021; Silva et al., 2025). The interaction between high aerosol loading and warm clouds—known as the aerosol indirect effect—remains a critical uncertainty in regional weather modification and hydrological cycles.

According to the theory of aerosol-cloud interactions, an increase in CCN concentration leads to a higher number of cloud droplets with smaller

**Citation:** Chantraket P, Danpradit S. Impact of biomass burning aerosols on warm cloud microphysics and rain suppression in Northern Thailand. Environ. Nat. Resour. J. 2027;25(X):xx-xx.

effective radii, assuming constant liquid water content (Twomey, 1977; Andreae et al., 2004). In warm cumulus clouds, this reduction in droplet size suppresses the collision-coalescence process (Tao et al., 2012), which is the primary mechanism for rain formation. Observational studies suggest that droplets must reach a critical threshold radius of ~14 μm (or diameter ~28 μm) to initiate effective collision-coalescence (Freud and Rosenfeld, 2012). In highly polluted environments, the abundance of aerosols creates a "microphysical bottleneck," preventing droplets from crossing this threshold and thereby inhibiting the onset of warm rain (Rosenfeld et al., 2008).

While previous studies in Northern Thailand have provided valuable baseline data, they have primarily focused on seasonal bulk characteristics. For instance, Chantraket et al. (2013) characterized the aerosol size spectra during the summer haze, identifying biomass burning from agricultural residues and wildfires as the primary sources driving high accumulation-mode concentrations. Subsequently, Chanyatham et al. (2016) investigated CCN properties and reported exceptionally high Twomey "k" parameters (up to 4.4) during pollution episodes, indicating a regime where droplet activation is highly sensitive to supersaturation variations. However, most of these investigations relied on flight-averaged data. There remains a scarcity of in-situ airborne observations that directly link these aerosol physicochemical properties to the short-term temporal evolution of cloud microphysics.

This study addresses these gaps by presenting results from an intensive aircraft campaign over Northern Thailand. A comprehensive suite of in-situ probes (UHSAS, PCASP, FSSP) is utilized to characterize the full particle size spectrum, distinguishing between fresh and aged biomass burning plumes. A 'step-ladder' flight strategy was employed to track the temporal evolution of cloud turrets, allowing for a direct assessment of how aerosol loading impacts droplet growth, rain suppression, and cloud lifetime.

## 2. METHODOLOGY

### 2.1 Study area and case selection

The observational data presented in this study were collected during an intensive field campaign conducted over the upper northern region of Thailand. The measurement period spanned from late February to mid-May 2024, capturing the transition from the peak biomass burning season to the pre-monsoon season. Flight operations were carried out using the Super King Air 350 research aircraft operated by the Department of Royal Rainmaking and Agricultural Aviation (DRRAA).

To ensure the analysis focused on active warm cloud formation potential, daily flight plans were determined based on morning radiosonde soundings. Potential cloud occurrence days were screened using the following criteria: (1) relative humidity (RH) greater than 60% in the sub-cloud layer as this threshold provides suitable atmospheric moisture conditions for cumulus cloud development (Adulyadej, 2005; Danpradit, 2020) and at the typical cloud base altitude (approximately 5,000-8,000 ft MSL); (2) thermodynamic instability indicated by negative values of the Showalter Index (SI) and Lifted Index (LI) (Detyothin et al., 2013; Chantraket et al., 2015; Royal Rainmaking Academic Group, 2021; Royal Rainmaking Academic Group, 2023); and (3) wind speeds less than 20 knots (Royal Rainmaking Academic Group, 2021; Royal Rainmaking Academic Group, 2023) to ensure stable in-situ sampling. Based on these criteria, nine distinct warm cumulus cloud cases (C1-C9) were selected for detailed analysis. The general characteristics of each case are summarized in Table 1.

### 2.2 Aircraft instrumentation

In-situ measurements of aerosol and cloud microphysical properties were conducted using a comprehensive suite of airborne instruments recording at a frequency of 1 Hz with a time resolution of 1 s. The characteristics of the particle size distribution (PSD) were measured using three complementary optical probes:

- Ultra-High Sensitivity Aerosol Spectrometer (UHSAS, DMT Inc, USA): Used to measure fine aerosol particles in the diameter range of 0.06 μm to 1.0 μm. In this study, UHSAS data were specifically utilized to characterize the Aitken mode ($0.06 \leq D < 0.1$ μm).
- Passive Cavity Aerosol Spectrometer Probe (PCASP-100X, DMT Inc, USA): Used to measure aerosols in the range of 0.1 μm to 1.0 μm, providing data for the Accumulation mode.
- Cloud Droplet Probe (FSSP-100, DMT Inc, USA): Used to measure cloud droplets in the range of 1.0 μm to 50 μm.

**Table 1.** General characteristics of the nine selected warm cloud cases, including location, timing, and cloud dimensions

| Case | Date | Time (LST) | Location (Lat, Lon) | Area (Province) | Base (ft) | Top (ft) | Depth (ft) | Diameter (km) | RH (ML) (%) | Winddi. (5-10 kft.) | Windspeed 5-10 kft. (knot) | LI | SI |
|---|---|---|---|---|---|---|---|---|---|---|---|---|---|
| C1 | 28 Feb | 14:51-15:41 | 18.5898°N, 100.0899°E | Lampang | 7,000 | 13,000 | 6,000 | 5 | 64 | 229 | 11 | -2.30 | -0.43 |
| C2 | 05 May | 14:09-15:00 | 17.6190°N, 100.8773°E | Phitsanulok | 8,000 | 11,000 | 3,000 | 3 | 64 | 248 | 04 | -4.45 | -4.04 |
| C3 | 08 May | 13:44-14:39 | 17.3495°N, 100.5011°E | Phitsanulok | 5,500 | 9,000 | 3,500 | 7 | 87 | 192 | 06 | -1.10 | -2.56 |
| C4 | 09 May | 14:02-14:58 | 15.6224°N, 99.4781°E | Nakhon Sawan | 7,000 | 11,000 | 4,000 | 6 | 74 | 177 | 03 | -4.76 | -3.59 |
| C5 | 10 May | 13:43-14:49 | 17.9075°N, 99.8982°E | Phrae | 7,000 | 10,000 | 3,000 | 3 | 78 | 223 | 09 | -2.88 | -2.35 |
| C6 | 13 May | 13:58-14:29 | 15.8122°N, 101.0900°E | Phetchabun | 6,500 | 10,000 | 3,500 | 5 | 76 | 199 | 03 | -3.53 | -3.77 |
| C7 | 14 May | 13:18-14:07 | 15.6606°N, 101.2303°E | Phetchabun | 4,500 | 9,000 | 4,500 | 6 | 84 | 270 | 04 | -1.17 | -2.25 |
| C8 | 17 May | 12:51-14:02 | 15.9774°N, 100.8490°E | Phetchabun | 4,000 | 8,000 | 4,000 | 5 | 85 | 213 | 12 | -3.11 | -1.71 |
| C9 | 18 May | 13:45-14:27 | 15.7998°N, 101.1199°E | Phetchabun | 4,500 | 8,500 | 4,000 | 2 | 87 | 231 | 08 | -0.80 | -0.14 |

Note: Data were obtained from the radiosonde soundings of the Rong Kwang Radar Station, Phrae Province, Thailand. The data were processed using the Thailand Cumulus Modeling method (Detyothin et al., 2018).

Additionally, CCN concentrations were measured using a CCN counter operating at a constant supersaturation of 0.5%. Bulk cloud water content was derived from a hot-wire liquid water content sensor (NEVP). State parameters (temperature, pressure, humidity, and wind vector) were measured by the Aircraft Integrated Meteorological Measurement System (AIMMS-20). The specifications of the instrumentation are summarized in Table 2. Instruments were routinely calibrated and maintained according to standard operational guidelines.

### 2.3 Warm cloud event data selection

For this study, warm cloud events occurring in northern Thailand during the summer season of 2024 (February to May) were meticulously selected. The screening process was applied to a specific subset of cloud sampling records, from which nine distinct cases were identified. These selection criteria were defined based on long-term operational observations of warm cloud climatology in Thailand to ensure the isolation of representative, non-precipitating, single-cell cumulus clouds selected through visual inspection:

1. Horizontal Dimension: The cloud must be a single-cell cumulus with a diameter of at least 2 kilometers.
2. Vertical Extent: The cloud's vertical thickness must exceed 2,000 feet, and its cloud top must be confined below the freezing level (approximately 16,000 feet MSL).
3. Precipitation-Free Vicinity: There must be no detectable rainfall within a 10-kilometer radius of the sample cloud to ensure the isolation of non-precipitating targets.

**Table 2.** Specifications of the airborne instrumentation installed on the DRRAA research aircraft

| Instrument | Parameter measurement | Measurement range | Application in this study |
|---|---|---|---|
| UHSAS | Fine Aerosol Size Dist. | 0.06-1.0 µm | Aitken Mode (0.06≤D<0.1 µm) |
| PCASP-100X | Aerosol Size Dist. | 0.1-3.0 µm | Accumulation Mode (0.1≤D<1.0 µm) |
| FSSP-100 | Cloud Droplet Size Dist. | 1.0-50 µm | Cloud Droplets (D≥1.0 µm) |
| CCNC | CCN Concentration | 0.75-10 µm | Measured at constant SS=0.5% |
| NEVP | Liquid Water Content | 0.05-3.0 g/m$^3$ | Bulk LWC measurement |
| AIMMS-20 | State Parameters | Standard Meteorological | T, P, RH, Wind Vector, Position |

### 2.4 Flight strategy

To investigate the aerosol-cloud interactions and track the short-term evolution of cloud microphysics, a "step-ladder" flight pattern was executed for each selected cloud case (Figure 1). The sampling strategy consisted of three primary legs:

1. Sub-cloud Leg (L1): A level traverse approximately 300 m (1,000 ft) below the cloud base to characterize the inflow aerosol properties and CCN concentration.
2. In-cloud Leg (T1): A penetration at ~300 m above the cloud base to capture the initial droplet activation and growth near the cloud base.
3. Evolution Leg (T2): A reciprocal penetration through the same cloud turret after a time interval ($\Delta t \approx 20$ min) to document the temporal evolution of the microphysical parameters.

### 2.5 Data processing

To characterize the full particle size spectrum from unactivated aerosols to cloud droplets, data from the optical probes were merged into a single composite distribution. The overlapping bins were removed to prevent double counting. The composite spectrum was derived by combining the UHSAS data for the Aitken mode range (0.06≤D<0.1 µm), the PCASP data for the accumulation mode range (0.1≤D<1.0 µm), and the FSSP data for the coarse mode range (D≥1.0 µm). This combination allows for a seamless analysis of the full evolution from fresh smoke particles to mature cloud droplets.

## 3. RESULTS AND DISCUSSION

### 3.1 Sub-cloud aerosol characteristics: Signatures of plume aging

To classify the origin of the aerosol air masses encountered during the campaign, 24-hour backward trajectories were computed using the NOAA HYSPLIT model (Stein et al., 2015; Sresawasd et al., 2021; Paluang et al., 2026), initialized with meteorological fields from the Global Data Assimilation System (GDAS). Figure 2 illustrates the transport pathways for the representative cases.

- Fresh Plume (Case C5): The trajectory (Figure 2(b)) indicates a stagnant air mass with localized recirculation over the sampling area within

the preceding 24 hours. This suggests that the aerosols were freshly emitted from local biomass burning sources with minimal atmospheric aging.

- Aged Plume (Case C1): In contrast, the trajectory (Figure 2(d)) reveals directional transport from the border regions (e.g., Myanmar), passing over complex terrain before reaching the study site. This suggests the presence of aged smoke plumes that have undergone atmospheric processing.

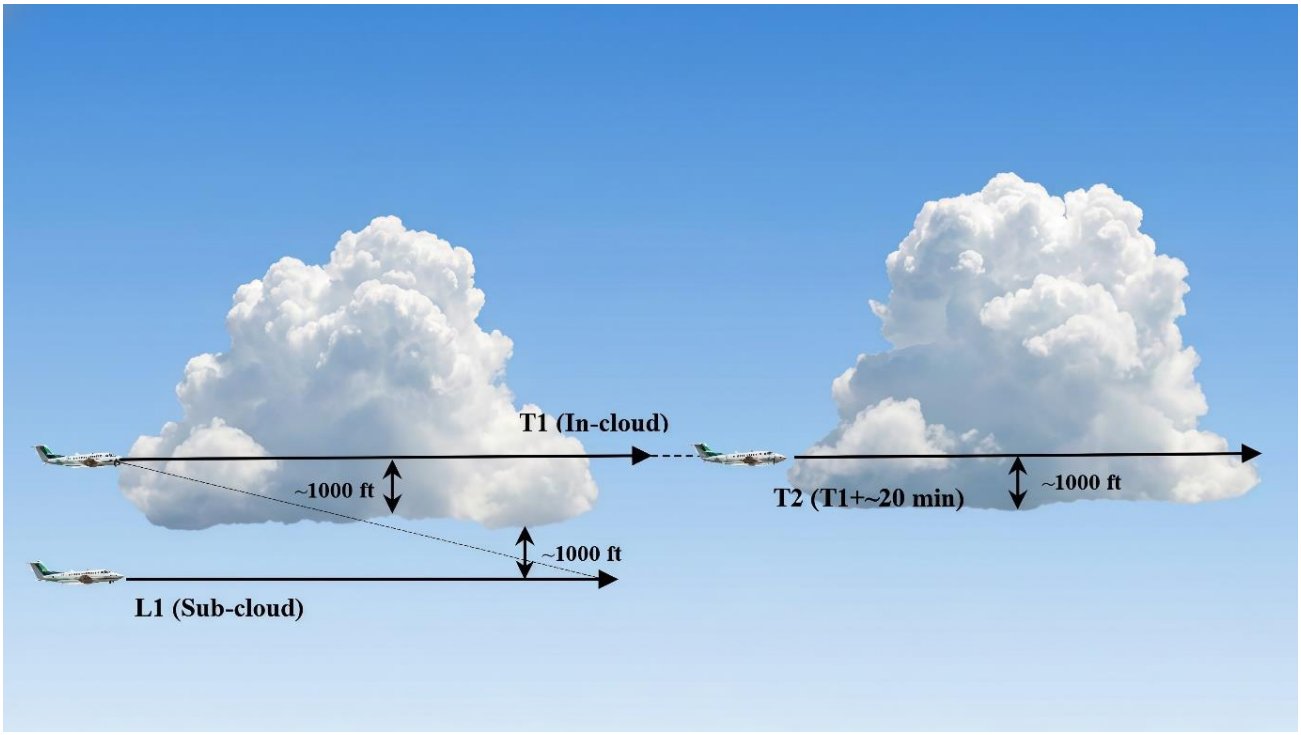



**Figure 1.** Schematic diagram illustrating the "step-ladder" flight strategy employed for observing cloud evolution. The flight path includes a sub-cloud aerosol sampling leg (L1), followed by an initial cloud penetration (T1) near the cloud base, and a subsequent re-penetration (T2) of the same cloud turret after a time interval of $\Delta t \approx 20$ minutes.

These distinct transport histories are supported by the in-situ microphysical measurements shown in Figure 3. The composite aerosol size distributions (PSD), constructed by merging data from UHSAS, PCASP, and FSSP, reveal distinct microphysical properties that govern the sub-cloud layer.

Case C5 (Fresh Plume, green line) exhibits a dominant mode in the ultrafine size range (<0.1 µm), captured by the UHSAS. This high concentration of Aitken-mode particles suggests active nucleation and recent emissions from local fires, consistent with the characteristics of fresh biomass burning aerosols described by Reid et al. (2005). In contrast, Case C1 (Aged Plume, blue line) shows a suppressed Aitken mode but a pronounced peak in the accumulation mode (0.1-0.3 µm). This shift to larger sizes is attributed to coagulation and condensation processes occurring as the plume ages and is transported over the region (Janicot et al., 2008). These observations indicate that Northern Thailand is influenced by a complex mixture of local fresh emissions and transported aged haze, both of which contribute to the exceptionally high CCN loading available for cloud ingestion.

The relationship between the composite aerosol population ($D \geq 0.1$ µm) and CCN activity, summarized in Table 3, provides further insight into the plume characteristics. These observations indicate that Northern Thailand is influenced by a complex mixture of local fresh emissions and transported aged haze. This high aerosol loading is often confined within the boundary layer by strong temperature inversions typical of the region's topography, as previously documented by vertical profile analyses in Chantraket et al. (2013), which further limits the availability of CCN for cloud uptake.

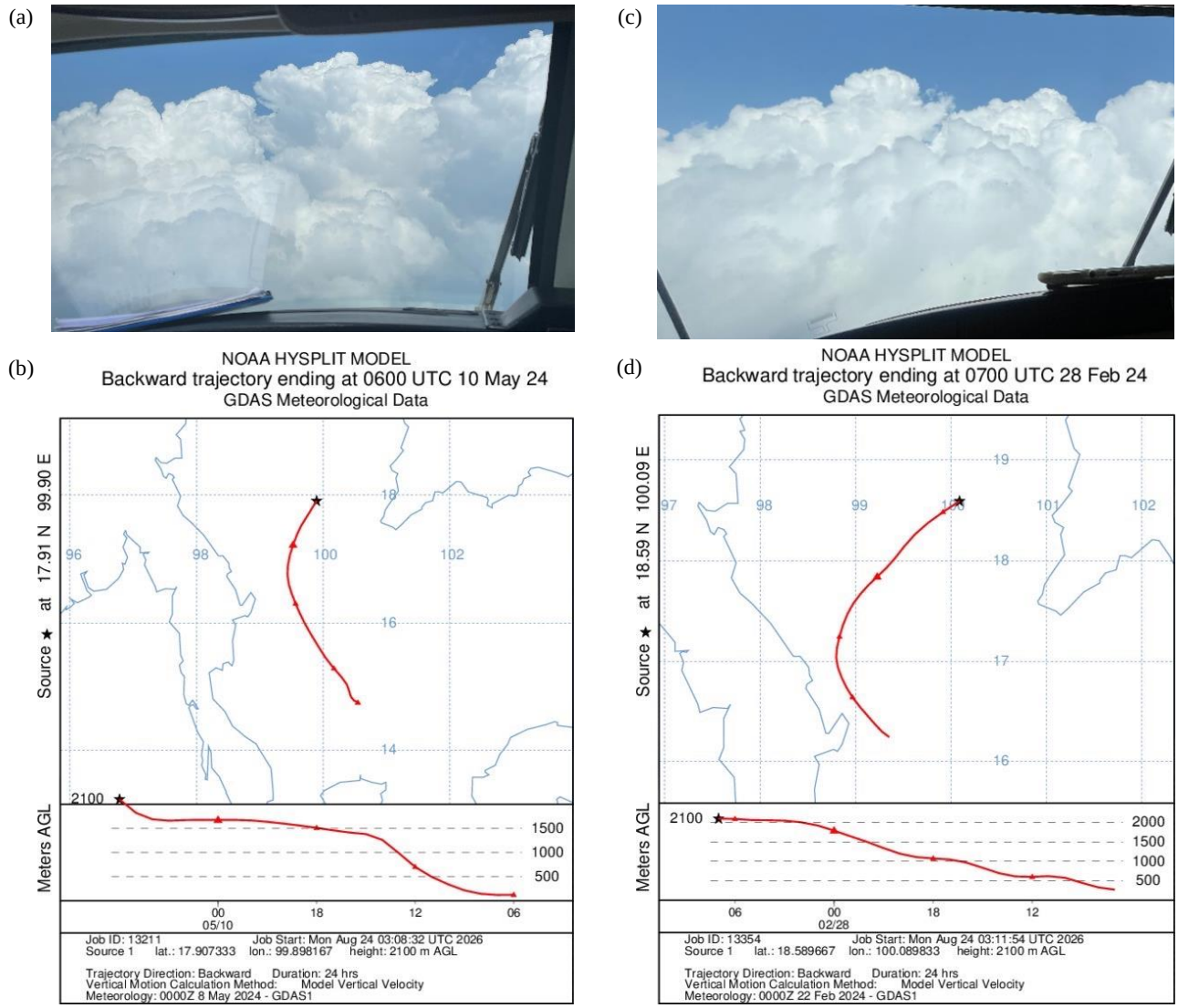



**Figure 2.** Comparison of cloud morphology and air mass trajectories between fresh and aged plumes: (a) Photograph of the sampled cloud for Case C5 (Fresh plume); (b) Corresponding 24-hour HYSPLIT backward trajectory for Case C5 indicating local recirculation; (c) Photograph of the sampled cloud for Case C1 (Aged plume); (d) Corresponding 24-hour HYSPLIT backward trajectory for Case C1 indicating directional transport

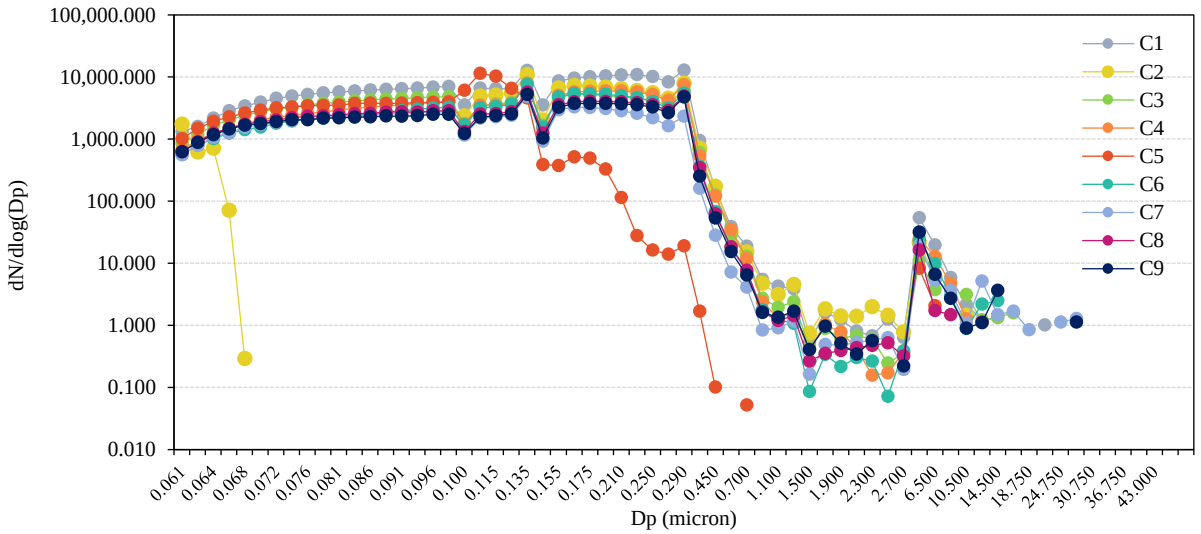



**Figure 3.** Composite sub-cloud particle size distributions (dN/dlog Dp) combining data from UHSAS, PCASP, and FSSP. Note the prominence of the Aitken mode in the fresh plume (Case C5) versus the accumulation mode in the aged plume (Case C1).

**Table 3.** Summary of sub-cloud environmental conditions, CCN concentrations (SS=0.5%), and total aerosol concentrations (Na) derived from PCASP and FSSP (D≥0.1 µm) for the nine sampled cases.

| Case | Date | ZBase (m) | TBase (ºC) | CCN 0.5% ($cm^{-3}$) | Na (D≥0.1µm) | Na (D≥0.5µm) | Ratio ($Na_{D\geq0.1\mu m}$/CCN) |
|---|---|---|---|---|---|---|---|
| C1 | 28 Feb | 2,134 | 17.7 | 4,901 | 5,549 | 22 | 1.13 |
| C2 | 05 May | 2,438 | 17 | 4,938 | 3,760 | 22 | 0.76 |
| C3 | 08 May | 1,676 | 22.6 | 2,839 | 2,788 | 16 | 0.98 |
| C4 | 09 May | 2,134 | 17.4 | 3,515 | 2,969 | 16 | 0.84 |
| C5 | 10 May | 2,134 | 18.5 | 2,540 | 3,155 | <1 | 1.24 |
| C6 | 13 May | 1,981 | 20.3 | 2,754 | 2,680 | 9 | 0.97 |
| C7 | 14 May | 1,372 | 22.9 | 2,077 | 1,623 | 4 | 0.78 |
| C8 | 17 May | 1,219 | 24 | 2,095 | 1,967 | 8 | 0.94 |
| C9 | 18 May | 1,372 | 23.7 | 2,123 | 1,965 | 7 | 0.93 |
| Mean | - | 1,829 | 20.5 | 3,087 | 3,331 | 14 | 0.95 |

Note: Na represents the total concentration of particles calculated by summing measurements from PCASP and FSSP probes.

### 3.2 In-cloud microphysics and suppression of collision-coalescence

Despite the abundance of potential CCN, the conversion of cloud water into precipitation-sized droplets was found to be highly inefficient. Figure 4 presents the in-cloud particle size distributions measured during the initial penetration ($T_1$). A striking feature across all nine sampled cases is the extremely narrow width of the droplet spectra. The mean volume diameters ($D_{mean}$) were consistently confined to the range of 2.0-4.0 µm.

Crucially, the droplet size distributions exhibit a sharp spectral cutoff at approximately 15-18 µm. No significant concentration of droplets larger than 20 µm was detected in any of the sampled clouds. This observed cutoff does not reach the critical threshold radius of ~14 µm (diameter ~28 µm) required for effective collision-coalescence (Freud and Rosenfeld, 2012), suggesting that the high aerosol loading effectively creates a microphysical bottleneck (Chen et al., 2021).

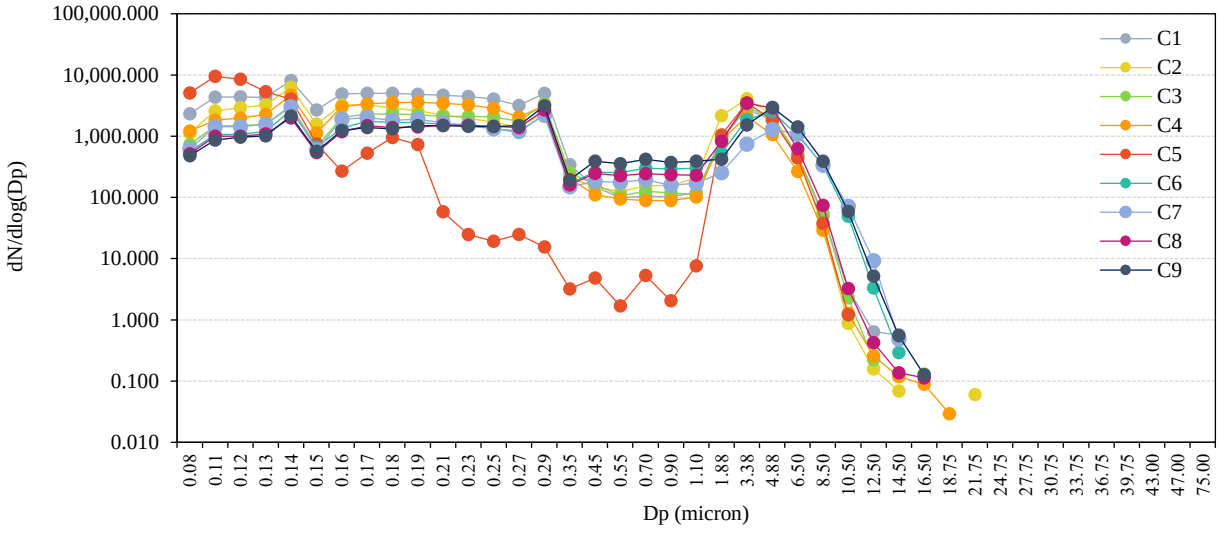



**Figure 4.** Composite in-cloud particle size distributions measured during the initial penetration (T1), combining data from PCASP, and FSSP. The spectra exhibit a sharp cutoff at 15-18 µm, indicating the suppression of collision-coalescence.

### 3.3 Temporal evolution and cloud dissipation mechanisms

To quantify the fate of these suppressed clouds, the temporal evolution of microphysical parameters was analyzed by conducting a second penetration ($T_2$) approximately 20 minutes after the initial sampling. The changes in Liquid Water Content (LWC), total

droplet concentration ($N_C$), and mean diameter ($D_{mean}$) are summarized in Table 4.

*3.3.1 Rapid evaporation and entrainment*

The dominant evolutionary trend observed in this study is rapid cloud dissipation. In 7 out of 9 cases, LWC decreased by 30-60% within the short observational interval (Table 4). The spectral analysis in Figure 5 shows a uniform reduction in droplet concentration across all size bins (dashed lines T2 vs. solid lines T1) without any spectral broadening. This suggests that mixing with dry environmental air (entrainment) is the governing process, eroding the cloud liquid water content and accelerating droplet evaporation before precipitation embryos can form (Small et al., 2009; Small et al., 2013; Yeom et al., 2025).

*3.3.2 The "cloud choking" effect (case C2)*

Case C2 presents a distinct and extreme scenario of aerosol-cloud interaction. As shown in Figure 5 (Panel C2) and Table 4, the cloud experienced a catastrophic collapse, with LWC dropping by 61% and droplet concentrations falling to near-background levels. This collapse coincided with a massive intrusion of aerosols, with the total concentration increasing by 233%, reaching peak values exceeding 7,700 $cm^{-3}$.

**Table 4.** Temporal evolution of cloud microphysical parameters between the initial (T1) and subsequent (T2) penetrations (Δt≈20 min).

| Case | Date | Evolution status | Δ LWC (%) | Δ Total conc. (%) | $\Delta D_{mean}$ (%) |
|---|---|---|---|---|---|
| C1 | 28/2 | Dissipating | -31.9 | +0.6 | -6.5 |
| C2 | 05/5 | Cloud Choking | -61.1 | +233.3 | -15.7 |
| C3 | 08/5 | Dissipating | -59.6 | -6.2 | -22.3 |
| C4 | 09/5 | Dissipating | -60.9 | -7.0 | -8.8 |
| C5 | 10/5 | Sustaining | +12.8 | -4.5 | -1.5 |
| C6 | 13/5 | Dissipating | -51.0 | -0.9 | -6.2 |
| C7 | 14/5 | Secondary Act | +52.3 | +4.6 | -22.9 |
| C8 | 17/5 | Dissipating | -42.1 | -2.3 | -3.9 |
| C9 | 18/5 | Dissipating | -47.6 | -15.4 | -19.3 |

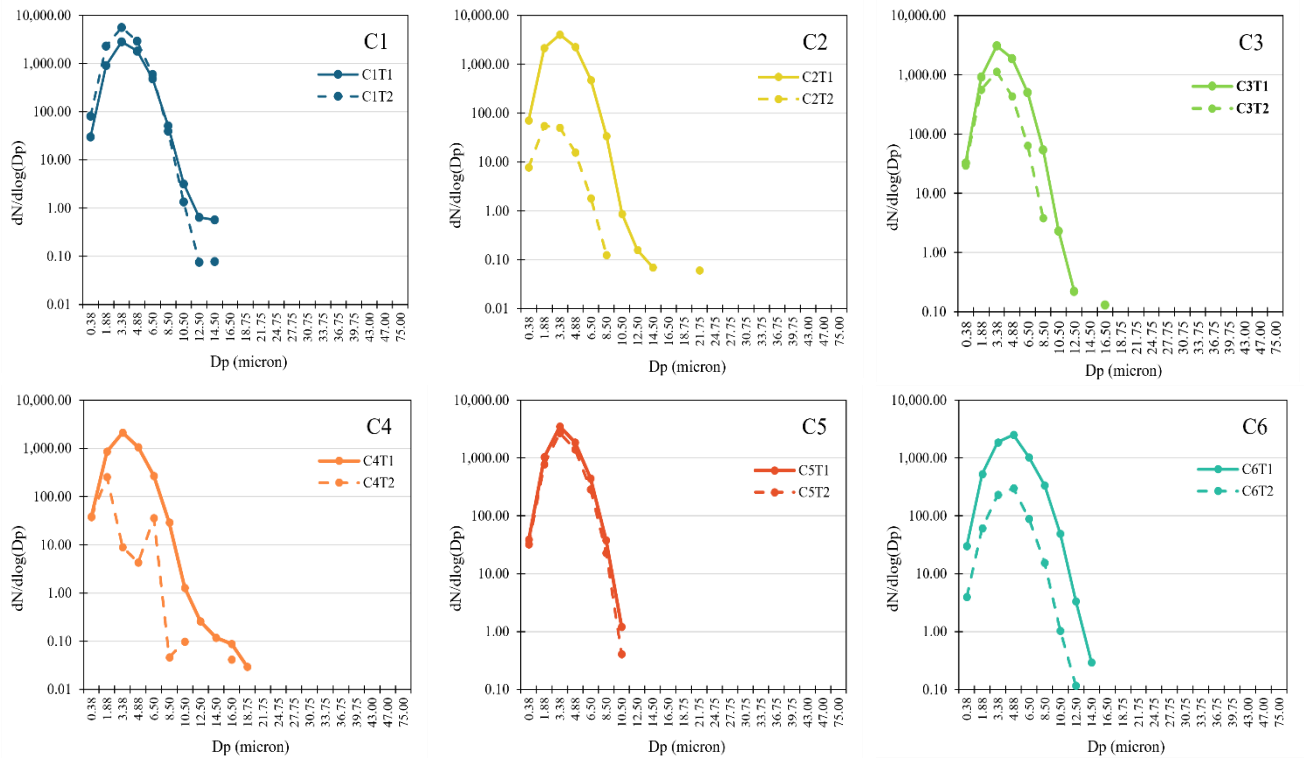



**Figure 5.** Temporal evolution of cloud droplet size distributions for the nine sampled cases. Solid lines represent the initial penetration (T1), and dashed lines represent the subsequent penetration (T2). The spectral collapse in most cases (e.g., C2, C3, C4) highlights rapid cloud dissipation.

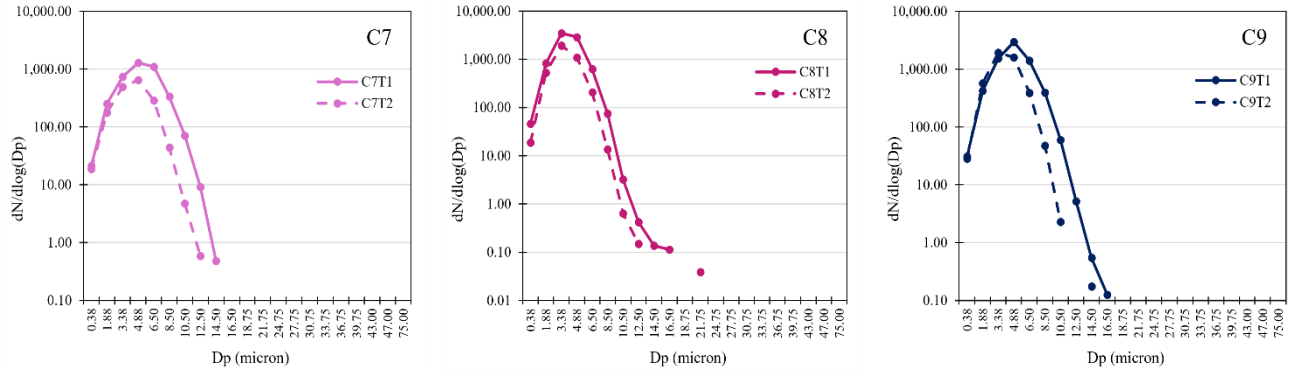



**Figure 5.** Temporal evolution of cloud droplet size distributions for the nine sampled cases. Solid lines represent the initial penetration (T1), and dashed lines represent the subsequent penetration (T2). The spectral collapse in most cases (e.g., C2, C3, C4) highlights rapid cloud dissipation. (cont.)

This inverse relationship—increasing aerosol loading leading to rapid cloud dissipation—provides direct in-situ evidence of the "semi-direct effect" (Ackerman et al., 2000; Lin et al., 2026). In this mechanism, the absorption of solar radiation by dark, carbonaceous smoke particles warms the air within or around the cloud, reducing relative humidity and increasing the evaporation rate. This "cloud choking" phenomenon effectively burns off the cloud, further suppressing any potential for precipitation (Roberts et al., 2003; Koren et al., 2004; Koch and Delgenio, 2010; Dagan et al., 2016).

*3.3.3 Secondary activation and growth stagnation*

Even in cases where the cloud remained dynamically active, such as Case C7 which exhibited strong updrafts Wmax ~ 4.0 m/s and a 52% increase in LWC, droplet growth was not observed. Instead, the mean droplet diameter decreased by 23% (Table 4). This indicates that the strong vertical velocity in this high-aerosol environment triggered secondary activation of fresh, small CCN, rather than promoting the growth of existing droplets. This observation aligns well with the hygroscopicity findings of Chanyatham et al. (2016), who reported extremely high Twomey "k" values (k≈3.8-4.4) for this region during the burning season. Such high k values imply that the CCN population is dominated by small, less hygroscopic particles that require high supersaturations to activate. Consequently, when updrafts strengthen, these numerous small particles are suddenly activated, flooding the cloud with tiny droplets and effectively shutting down the spectral broadening process.

## 4. CONCLUSION

This study provides comprehensive in-situ observational evidence of warm rain suppression mechanisms over the biomass-burning region of Northern Thailand. Integrating analysis from HYSPLIT trajectories, full-spectrum aerosol measurements (UHSAS, PCASP, FSSP), and cloud evolution tracking leads to three primary conclusions:

1. Dual Aerosol Regimes: The sub-cloud layer is characterized by a complex mixture of aerosols. Distinct microphysical signatures were identified for fresh plumes, dominated by the Aitken mode (<0.1 µm) and originating from local stagnant recirculation, and aged plumes, dominated by the accumulation mode (0.1-0.3 µm) and associated with long-range transport.

2. Both regimes contribute to an excessively high CCN background available for cloud ingestion.

3. Suppression of Precipitation: The high aerosol loading imposes a severe microphysical barrier to rain formation. Despite the availability of moisture, the competition for water vapor limits droplet growth, creating a "bottleneck" at 15-18 µm. Consequently, the collision-coalescence process is effectively shut off, preventing the formation of precipitation-sized droplets (>20 µm).

4. Shortened Cloud Lifetime: The dominant fate of these warm clouds is rapid dissipation. The tracking analysis revealed that Liquid Water Content (LWC) typically decreased by 30-60% within 20 minutes. This decay is driven primarily by dry air entrainment and, in extreme pollution events, by the "semi-direct effect" (cloud choking), where massive aerosol intrusion accelerates droplet evaporation.

These findings underscore that under current atmospheric conditions during the haze season, natural

warm rain formation is highly inefficient. The results highlight the critical need for targeted weather modification strategies to overcome these microphysical barriers and mitigate the hydrological impacts of aerosol pollution.

## ACKNOWLEDGEMENTS

This research incorporates data from the Pilot Project on Weather Modification for Air Pollution Mitigation by Cloud Scavenging, a project supported by the Thailand Science and Innovation Research Institute (TSRI), and data from aerial operations conducted by the Department of Rainmaking and Agricultural Aviation.

## AUTHOR CONTRIBUTIONS

Conceptualization, C.P.; Methodology, D.S.; Experimentation, D.S.; Conducted the data analysis, C.P.; Writing-Original Draft Preparation Review and Editing C.P.

## DECLARATION OF CONFLICT OF INTEREST

The authors declare no competing financial or personal interests that could have influenced the work reported in this paper.

## REFERENCES

Ackerman AS, Toon OB, Stevens DE, Heymsfield AJ, Ramanathan V, Welton EJ. Reduction of tropical cloudiness by soot. Science 2000;288(5468):1042-7.

Adulyadej B. Weather Modification by Royal Rainmaking Technology. European patent EP1491088B1. European Patent Office; 2005.

Amnuaylojaroen T, Inkom J, Janta R, Surapipith V. Long range transport of Southeast Asian $PM_{2.5}$ pollution to northern Thailand during high biomass burning episodes. Sustainability 2020;12(23):Article No. 10049.

Andreae MO, Rosenfeld D, Artaxo P, Costa AA, Frank GP, Longo KM, et al. Smoking rain clouds over the Amazon. Science 2004;303(5662):1337-42.

Bran SH, Macatangay R, Chotamonsak C, Chantara S, Surapipith V. Understanding the seasonal dynamics of surface $PM_{2.5}$ mass distribution and source contributions over Thailand. Atmospheric Environment 2024;331:Article No. 120613.

Chantraket P, Kirtsaeng S, Detyothin C, Nakburee A, Mongkala K. Characteristics of hailstorm over northern Thailand during summer season. EnvironmentAsia 2015;8(1):101-14.

Chantraket P, Tantiplubthong N, Chanyatham T. Aerosol and cloud condensation nuclei distribution during summer season over northern region of Thailand. Journal of Environmental Research 2013;35(1):87-102.

Chanyatham T, Chantraket P, Tantiplubthong N. Observations of cloud condensation nuclei (CCN) in northern Thailand. Chiang Mai Journal of Science 2016;43(4):767-76.

Chen YC, Wang SH, Min Q, Lu S, Lin PL, Lin NH, et al. Aerosol impacts on warm-cloud microphysics and drizzle in a moderately polluted environment. Atmospheric Chemistry and Physics 2021;21(6):4487-502.

Dagan G, Koren I, Altaratz O, Heiblum RH. Aerosol effect on the evolution of the thermodynamic properties of warm convective cloud fields. Scientific Reports 2016;6:Article No. 38769.

Danpradit S, Budmuang R, Butsabong C, Boonchouy S, Nakburee A, Leenanon J, et al. Influence of Cloud Microphysics Properties of Sub-cloud Layer on Cumulus Clouds. Bangkok, Thailand: Department of Royal Rainmaking and Agricultural Aviation; 2020 (in Thai).

Detyothin C, Chantraket P, Nakburee A. The Development of Upper-Air Thailand Cumulus Modeling (TCM): Case Study—Upper Northern, Central, Eastern, and Northeastern Parts of Thailand. Proceedings of the 21st Conference on Planned and Inadvertent Weather Modification; 2018 Jan 7-11; Austin, Texas: United States of America; 2018.

Detyothin C, Chantraket P, Sooknarint A, Chanyatham T, Polharn T, Srisathittham P, et al. The Study of the Development of Upper Air Observation Forecasting System for Using Rainmaking Operation Case Study Upper Northern of Thailand. Bangkok, Thailand: Department of Royal Rainmaking and Agricultural Aviation; 2013 (in Thai).

Freud E, Rosenfeld D. Linear relation between convective cloud drop number concentration and depth for rain initiation. Journal of Geophysical Research: Atmospheres 2012; 117(D2):Article No. D02207.

Inlaung K, Chotamonsak C, Macatangay R, Surapipith V. Assessment of transboundary $PM_{2.5}$ from biomass burning in northern Thailand using the WRF-Chem model. Toxics 2024;12(7):Article No. 462.

Jainontee K, Pongkiatkul P, Wang YL, Weng RJF, Lu YT, Wang TS, et al. Strategy design of $PM_{2.5}$ controlling for northern Thailand. Aerosol and Air Quality Research 2023; 23(6):Article No. 220432.

Janicot S, Thorncroft CD, Ali A, Asencio N, Berry G, Bock O, et al. Large-scale overview of the summer monsoon over West Africa during the AMMA field experiment in 2006. Annales Geophysicae 2008;26(9):2569-95.

Kawichai S, Prapamontol T, Cao F, Song W, Zhang YL. Characteristics of carbonaceous species of $PM_{2.5}$ in Chiang Mai City, Thailand. Aerosol and Air Quality Research 2024;24(4):Article No. 230269.

Koch D, Del Genio AD. Black carbon semi-direct effects on cloud cover: Review and synthesis. Atmospheric Chemistry and Physics 2010;10(16):7685-96.

Koren I, Kaufman YJ, Remer LA, Martins JV. Measurement of the effect of Amazon smoke on inhibition of cloud formation. Science 2004;303(5662):1342-5.

Lin PH, Wang SH, Klemm O, Lin NH. Separating the Twomey effect and the semi-direct effect in absorbing aerosol environments through the cloud-aerosol mixing ratio. Atmospheric Chemistry and Physics 2026;26(3):2083-102.

Luong ND, Chuersuwan N, Viet HT, Trung BQ. Impact of biomass burning sources during the high season on $PM_{2.5}$ pollution observed at sampling sites in Hanoi, Vietnam and Chiang Rai, Thailand. APN Science Bulletin 2022;12(1):56-65.

Paluang P, Chetiyanukornkul T, Suriyawong P, Furuuchi M, Phairuang W. Assessment of urban size-fractionated PM down to $PM_{0.1}$ influenced by daytime and nighttime open biomass fires in Chiang Mai, northern Thailand. Urban Science 2026;10(2):Article No. 103.

Reid JS, Koppmann R, Eck TF, Eleuterio DP. A review of biomass burning emissions part II: Intensive physical properties of biomass burning particles. Atmospheric Chemistry and Physics 2005;5(3):799-825.

Roberts GC, Nenes A, Seinfeld JH, Andreae MO. Impact of biomass burning on cloud properties in the Amazon Basin. Journal of Geophysical Research: Atmospheres 2003;108(D2):Article No. 4062.

Rosenfeld D, Lohmann U, Raga GB, O'Dowd CD, Kulmala M, Fuzzi S, et al. Flood or drought: How do aerosols affect precipitation? Science 2008;321(5894):1309-13.

Royal Rainmaking Academic Group. After Action Review Report of the 2021 Royal Rainmaking Operations. Bangkok, Thailand: Department of Royal Rainmaking and Agricultural Aviation; 2021 (in Thai).

Royal Rainmaking Academic Group. After Action Review Report of the 2023 Royal Rainmaking Operations. Bangkok, Thailand: Department of Royal Rainmaking and Agricultural Aviation; 2023 (in Thai).

Saksakulkrai S, Chantara S, Shi Z. Airborne particulate matter in Southeast Asia: a review on variation, chemical compositions and source apportionment. Environmental Chemistry 2023;19(7):401-31.

Silva KMR, Herdies DL, Kubota PY, Bresciani C, Figueroa SN. Impact of aerosols on cloud microphysical processes: A theoretical review. Geosciences 2025;15(8):Article No. 312.

Small JD, Chuang PY, Feingold G, Jiang H. Can aerosol decrease cloud lifetime? Geophysical Research Letters 2009;36(16):Article No. L16806.

Small JD, Chuang PY, Jonsson H. Microphysical imprint of entrainment in warm cumulus. Tellus B: Chemical and Physical Meteorology 2013;65(1):Article No. 19922.

Sresawasd C, Chetiyanukornkul T, Suriyawong P, Tekasakul S, Furuuchi M, Hata M, et al. Influence of meteorological conditions and fire hotspots on $PM_{0.1}$ in Northern Thailand during strong haze episodes and carbonaceous aerosol characterization. Aerosol and Air Quality Research 2021;21:Article No. 210069.

Stein AF, Draxler RR, Rolph GD, Stunder BJB, Cohen MD, Ngan F. NOAA's HYSPLIT atmospheric transport and dispersion modeling system. Bulletin of the American Meteorological Society 2015;96(12):2059-77.

Tao WK, Chen JP, Li Z, Wang C, Zhang C. Impact of aerosols on convective clouds and precipitation. Reviews of Geophysics 2012;50(2):Article No. RG2001.

Twomey S. The influence of pollution on the shortwave albedo of clouds. Journal of the Atmospheric Sciences 1977;34(7): 1149-52.

Yeom JM, Fahandezh Sadi H, Anderson JC, Yang F, Cantrell W, Shaw RA. Cloud microphysical response to entrainment of dry air containing aerosols. npj Climate and Atmospheric Science 2025;8:Article No. 8.